Hindawi
Journal of Nanotechnology
Volume 2018, Article ID 9537454, 10 pages
https://doi.org/10.1155/2018/9537454

Hindawi

Research Article

Biosynthesis of Ultrasonically Modified Ag-MgO Nanocomposite and Its Potential for Antimicrobial Activity

Wasiu B. Ayinde,[1] **Mugera W. Gitari**,[1] **Munkombwe Muchindu**,[2] **and Amidou Samie**[3]

[1]*Environmental Remediation and Water Pollution Chemistry Group (ERWPCG), Department of Ecology and Resource Management, School of Environmental Sciences, University of Venda, Private Bag X5050, Thohoyandou 0950, Limpopo, South Africa*
[2]*Mintek, Advanced Materials Division, Nanotechnology Innovation Centre, Randburg, South Africa*
[3]*Molecular Parasitology and Opportunistic Infections Program, Department of Microbiology, School of Mathematical and Natural Sciences, University of Venda, Thohoyandou, South Africa*

Correspondence should be addressed to Wasiu B. Ayinde; twasiu33@gmail.com

Received 2 May 2018; Revised 17 July 2018; Accepted 2 August 2018; Published 29 August 2018

Academic Editor: Marco Rossi

This study reports a green synthesis route for a bilayered Ag-MgO nanocomposite using aqueous peel extract of *Citrus paradisi* (grapefruit red) under an accelerated uniform heating technique and its antibacterial potency against *Escherichia coli*. Surface modifications and composition of the nanocomposite were examined using a UV-visible spectrophotometer, transmission electron microscopy (TEM), X-ray diffraction (XRD), Fourier-transform infrared (FTIR) spectroscopy, and scanning electron microscopy (SEM) equipped with an energy dispersive X-ray (EDX) analyzer. The efficiencies of the as-synthesized Ag-MgO nanocomposite against *Escherichia coli* were examined. The synthesized Ag-MgO nanocomposite showed characteristic synergetic bands at 290 nm for MgO nanoparticle and at around 440 nm for Ag nanoparticle which blue-shifted to 380 nm in the composite. A spherically dispersed nanocomposite with cubical crystal lattice network with a diameter of about 20–100 nm comprising Ag nanoparticle embedded within MgO nanoparticles was obtained. The nanocomposite produced stronger antibacterial activity against *Escherichia coli* as compared to MgO nanoparticle, indicating a higher interaction between Ag and MgO ions. The nanocomposite was successfully synthesized via an efficient modified method by bioreductive agents with an improved synergistic antibacterial property towards water purification.

1. Introduction

Waterborne epidemics associated with high faecal contamination by pathogenic microbes are a worldwide problem. The treatment of infectious water-related diseases is becoming a threat to human existence because of the increase in some high resistance to the causative microbial agent. The consequence is a potential public health threat due to an epidemic outbreak of diseases often associated with microbiological contamination, resulting in an increasing number of deaths across the globe, mostly among children [1]. Water disinfection through the use of conventional methods such as chlorination and ultraviolet (UV) irradiation is rapidly becoming a major challenge due to the formation of harmful carcinogenic disinfection byproducts (DBPs) [2, 3]. The development of inorganic nanoparticles with improved physicochemical and biological properties from the biosynthesized route is on the rise due to the growing need to develop environmentally benign technologies in material synthesis against infectious organisms. Generally, with the efforts to reduce generated hazardous waste, green synthesis and chemical processes are progressively integrating with modern developments in science and industry [4]. Researchers are exploiting the introduction of eco-friendly materials towards the development of novel improved antibacterial nanomaterials against multidrug-resistant human pathogens like *Escherichia coli*. *E. coli* is one of the deadly contaminants in drinking water. The nontoxicity and

environmental compatibility of biosynthesis agents, especially from various plant-derived extracts or components, make them reliable biosynthesis agents for metal and metal oxide nanoparticle synthesis [5–7].

Among the metallic and metal oxide nanoparticles, silver (Ag) and magnesium oxide (MgO) nanoparticles have been extensively reported to possess broad-spectrum antibacterial activities [8–11]. Silver nanoparticles are undoubtedly the most widely used inorganic nanoparticles with tremendous applications in the field of highly sensitive biomolecular detection and antibacterial activities [12–14]. MgO nanoparticles, on the other hand, have recently received greater attention because of their vast applications in biomedical materials, catalysis, and as absorbents [15–17]. However, based on the antibacterial properties of MgO nanoparticles having less potent bactericidal effect in comparison to silver-based antibacterial agents, efforts are now being channeled into the development of composite materials to exert strong synergistic antibacterial activity against infectious pathogens through chemical methods [9, 18, 19]. However, the use of such chemicals in nanosynthesized biomedical materials has been a major concern due to their high cost, toxic nature, and production of non-eco-friendly byproducts and nonbiodegradable stabilizing agents posing a danger to the environment and human beings [20–22].

To address this shortcoming, successive biosynthetic approaches using plants extracts have been explored and reported [23, 24]. The plant-based approaches have many advantages over chemical methods. According to previous investigations, the polyol components and the water-soluble heterocyclic components in these plants play a significant role in the reduction of metallic ions. They have proven to be effective capping and stabilizing agents for the nanoparticles with widespread technological and medicinal applications [25–27]. Silver and magnesium oxide nanoparticles have been synthesized using various plant extracts. The use of the extract of different biodiversity plants has been extensively reported and reviewed for silver nanoparticles [8]. Furthermore, MgO nanoparticles have been successfully synthesized through different plant species extract including *Swertia chirayita* leaf extract [16], *Clitoria ternatea* [28], and *Emblica officinalis* fruit extracts [29].

The peel of some fruits contains considerable amounts of minerals and vitamins, especially in citrus fruits. Previous studies have shown the presence of higher contents of phenolic, flavonoids, as well as other valuable secondary plant metabolites and essential oils in fruit peels than in other segments of citrus [30–32]. These metabolites are reported to account for various bioactivities including antibacterial and antioxidant properties [33, 34]. In addition to the eco-friendly application of these components in synthesizing nanoparticles, efforts are now focusing on identifying different novel energy transfer-assisted methods, such as microwave [35] and ultrasound [36], capable of providing efficient, uniform heating distribution in the formation of a stable and sustainable biomedical nanocomposite materials with improved physicochemical properties.

In this present study, *Citrus paradisi* (grapefruit red) peel extracts were used via an efficient heating medium towards its bioreducing, stabilizing, and capping ability in the formation of Ag-MgO nanocomposites. A detailed formation, characterization, and *E. coli* inactivation of the Ag-MgO nanocomposites were evaluated and reported. The novelty of this work is based on the fact that, to the best our knowledge, the use of aqueous *C. paradisi* peel extracts in biosynthesizing Ag-MgO and testing of its antibacterial activity have not been reported.

2. Materials and Methods

All chemicals were of analytical reagent grade. $Mg(NO_3)_2{\cdot}6H_2O$, $AgNO_3$, NaOH, and other chemicals used were purchased from Rochelle chemicals, South Africa, and used directly without further purification. Deionized water from Millipore (18.2 MΩ/cm) was used for the preparation and dilution of standards throughout the experiment.

2.1. Preparation of Citrus paradisi Peel Extracts. The fruit peels of *Citrus paradisi* (grapefruit red) were removed, cleaned thoroughly using ultrapure water (18.2 MΩ/cm) to remove any dust particles adhering to the surface, and cut into small pieces. 30 g of the peel was added to 100 mL of ultrapure water and boiled for 20 minutes at 70°C. The extract was cooled and filtered through Whatman no. 1 filter paper and stored at 4°C for further use.

2.2. Microwave-Assisted Synthesis of Silver Nanoparticles Using Citrus paradisi Peel Extract. Biosynthesized Silver nanoparticles (AgNps) were first obtained via the microwave-assisted sol-gel method. In a typical experiment, 40 mL of the filtrate of the citrus peel was added to 60 mL of 1 mM silver nitrate ($AgNO_3$) in 250 mL Erlenmeyer flasks at the ratio of 2 : 3 v/v for the reduction of Ag^+ to Ag^0. The mixture was then placed on a turntable domestic microwave oven (Russell Hobbs 20L (RHEM 21L)) operating at a power of 700 W and frequency of 2450 MHz at different time intervals of 30, 60, 90, 120, and 150 seconds for complete bioreduction. The formation of silver nanoparticles (AgNps) was monitored using UV-Vis Spectrophotometer over the wavelength range of 220–600 nm. Time-resolved absorption spectra of the UV-Vis spectroscopy were used in monitoring the periodic bioprocess growth kinetics of AgNps through color variation. The synthesized nanoparticle was used in subsequent experiments.

2.3. Synthesis of Ag-MgO Nanocomposite. Ag-MgO nanoparticles were synthesized by seed growth via the bioreduction route by the precipitation method at room temperature using a natural mild reducing agent (aqueous *Citrus paradisi* peel extracts) in the presence of the metallic precursors. 0.1 M·$Mg(NO_3)_2{\cdot}6H_2O$ and $1{\times}10^{-3}$ M $AgNO_3$ were used as the precursors of MgO and Ag, respectively.

In a typical experimental procedure, the Ag-MgO composite was obtained from an already optimized

microwave-assisted aqueous mixture of *C. paradisi* peel extracts (1 mM·$AgNO_3$ (2 : 3 v/v%)). 80 ml of this solution was mixed with 20 mL 0.1 M·$Mg(NO_3)_2$·$6H_2O$ under continuous stirring (2 h) at room temperature with 2 mL of 0.1 M·NaOH solution added dropwise until a complete precipitation was achieved. The composite solution was thereafter subjected to ultrasonic irradiation controlled at 100% amplitude (0.5 cycles) for 30 min. The product obtained was centrifuged (4500 rpm) for 30 min, filtered, and freeze-dried.

2.4. Physicochemical and Mineralogical Characterization of Synthesized Nanocomposite. The synthesized Ag and Ag-MgO nanomaterials absorption range was monitored using UV-visible spectrophotometer (SPECTROstar Nano/BMG LABTECH). Surface morphology of the nanoparticles was characterized using SEM (FEI Nova NanoSEM 230) with the field-emission gun equipped with an Oxford X-Max SDD detector operating at an accelerating voltage of 20 Kv for the EDS detector (Oxford X-Max with INCA software). The ALPHA FT-IR spectrophotometer from Bruker was used to obtain the FTIR spectra (4000–400 cm^{-1}). The crystalline phases present in the materials were identified by X-ray diffraction (X'Pert Pro; Cu-K radiation; wavelength 1.54443 Å). The transmission electron microscopy (TEM) image was taken using an FEI Tecnai 20 equipped with a LaB6 emitter, operating at 200 KV and fitted with a Gatan Tridiem GIF with a 2K×2K CCD camera. Images were collected using the digital micrograph suite of programs in relation to size and shape.

2.5. Antibacterial Evaluation of the Crude Extract and Nanomaterials. The bacterial resistance of the biosynthesized Ag-MgO nanocomposite, Ag, and MgO was determined from the observed zone of inhibition (mm) using the standard agar well disc diffusion methods (Kirby–Bauer disk diffusion test) and microdilution assay. The indicator strain used is *Escherichia coli* (ATCC 35218). Bacterial suspensions were prepared with the turbidity of 0.5 McFarland. 50 μL (1 mg/mL) of Ag, MgO, and Ag-MgO solution was impregnated on a cellulose nitrate sterile filter paper (pore size 0.45 μm) and allowed to dry at room temperature for 3 h and placed on MacConkey nutrient agar plates already inoculated with the bacterial cell suspension. The plates were incubated at 37°C for 24 h, and the diameter of the zone of growth inhibition around the sample was measured in millimeters (mm) and compared. The measured zones of inhibition were used to determine the antibacterial activities of the nanocomposite. Minimum inhibitory concentration (MIC) of biosynthesized Ag, MgO, and Ag-MgO was also determined using the microtiter broth-dilution method as described by Samie et al. [37].

2.6. Release of Silver and Magnesium Ions. To determine the release of silver and magnesium ions in solution, 1 mg/ml of the biosynthesized Ag-MgO was left to stand at room temperature for 3 h. At different time intervals, the suspension was collected and filtered through a membrane filter (pore size 0.45 μm (47 mm)). The concentrations of Ag-Mg ions in the filtrate (20 μL) were measured on PinAAcle 900T Atomic Absorption Spectrometer (AAS, PerkinElmer, Inc.).

3. Results and Discussion

3.1. Physicochemical and Mineralogical Characterization of Ag-MgO Nanocomposite

3.1.1. UV-Visible Analysis. Figures 1 and 2 show UV-visible absorbance spectra for the Ag nanoparticle and Ag-MgO nanocomposite. The successful bioreduction formation of AgNps by aqueous extract of *C. paradisi* peel extracts at a mixing ratio of 2 : 3 by volume at different time intervals ranging between 0–150 s under microwave irradiation is indicated by a change in the color of the reaction solution from light yellow to dark brown (Figure 1). AgNps were observed at intervals of 0–150 s with a characteristic surface plasmon vibration band ranging between 410 and 440 nm appearing at approximately 30 s of the reaction nucleation and onset of growth. The absorption peak intensity gradually increases with the increase of irradiation time with some overlapping plasmon bands with the formation of more AgNps evidently the same sizes which may be due to the stabilizing effect of the *C. paradisi* peel extract biomolecule. The intensity of the peaks indicated that *C. paradisi* peel extracts enhanced the bioreduction process of Ag^+ with the continual formation of AgNps up to 150 s with little variation in the absorption maxima. In general, the morphology of the nanoparticles is greatly influenced by the surface plasmon resonance, due to the mutual vibration of electrons of metal nanoparticles in resonance with light wave serving as the basis for measuring adsorption of the material onto the surface of metal nanoparticles [38, 39]. Furthermore, the use of microwaves is vital in the development of this nanoparticle because it is eco-friendly in nature and provides rapid and even heating of the reaction medium, thus offering uniform nucleation and growth conditions for nanoparticles within the short reaction time unlike the traditional external heating methods [40].

Figure 2 depicts an absorption spectrum of the synthesized biogenic Ag-MgO nanocomposite. As shown in the spectrum, two different distinct peaks were observed. A prominent intense band is observed in the low-UV region at 290 nm typical of MgO together with a broad band at 378 nm associated with AgNPs. It is observed that the incorporation of MgO onto the Ag layer resulted in a blue shift in the peak of AgNps from 440 nm to 378 nm. This shifting is attributed to its particle size, which depends on nucleation and growth mechanism based on the excitation of plasmon resonance or interband transition, particularly on the size effect [13]. This clearly indicates the reduction in the particle size resulting from the optical property of biomolecular capped Ag-MgO nanocomposite. Furthermore, the sizes of the composites were affected upon ultrasound exposure due to the cavitational collapse phenomenon resulting in an interparticle collision, thus affecting the physicochemical properties of

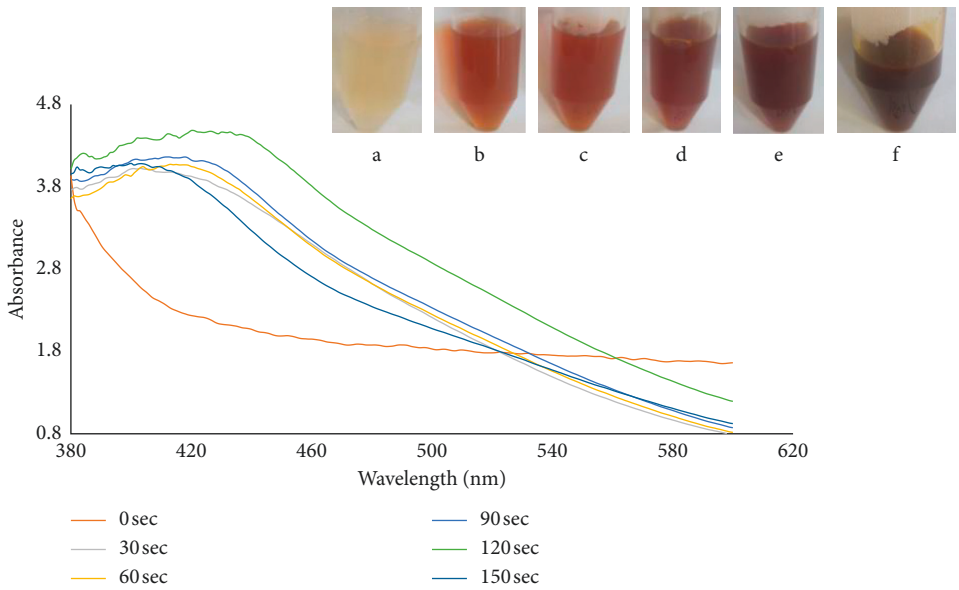

Figure 1: UV-visible spectra and photographic representation of silver nanoparticles biosynthesized by using aqueous *C. paradisi* peel extract at the mixing ratio of 2 : 3 at different time intervals.

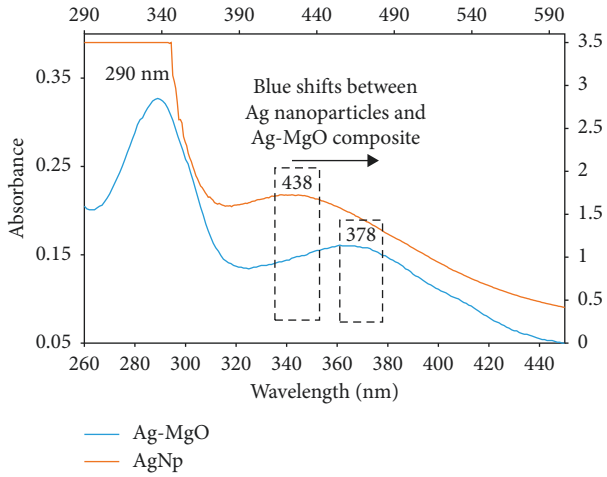

Figure 2: UV-visible spectra of biomolecular capped Ag-MgO nanocomposite.

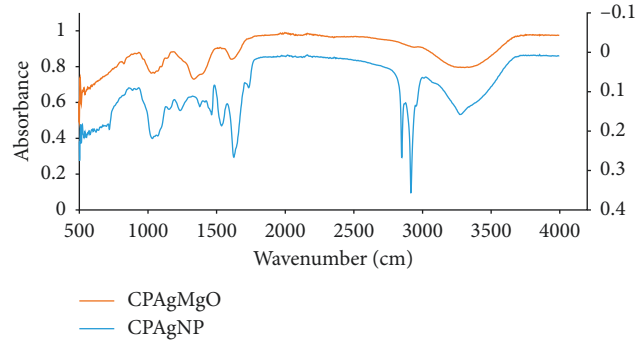

Figure 3: Comparative FTIR spectra of biosynthesized Ag and Ag-MgO nanomaterial.

the composite in relation to the incident frequency of the sonicator [41, 42]. It can be established that the availability and impacts of the phytochemicals in *C. paradisi* peel extracts were responsible for the rate of bioreduction leading to the formation of the composites.

3.1.2. FTIR Analysis. The functional groups of the various metabolites present in the *C. paradisi* peel extract responsible for the bioreduction, capping, and stabilizing of the Ag-MgO nanocomposite were identified between 4000 and 500 cm^{-1} of the FTIR region. Figure 3 shows the comparative FTIR spectra of as-synthesized Ag(CPAgNp) and Ag-MgO(CPAgMgO) from the aqueous *C. paradisi* peel extract. In the CPAgNp spectrum, a strong band centred at around 3282 cm^{-1} resulting from the stretching vibrations of the hydroxyl (–OH), N–H stretch of various metabolites present in the peel extract in the form of alcohol and N–H stretch of 1° and 2° amines or amides, carboxylic acid, ester, and ether [39]. These peaks shifted to a higher and broader frequency range of 3440–3200 cm^{-1} in intensity on binding with MgO in CPAgMgO nanocomposite. The sharp peaks observed at 2915 cm^{-1} and 2849 cm^{-1} in CPAgNps which disappeared in the CPAgMgO spectrum could be assigned to the symmetric and asymmetric C–H stretching vibrations of methyl, methylene, and methoxy groups [43, 44]. The presence of C=O is found in both spectrums at 1734 cm^{-1} and 1625 cm^{-1} for CPAgNps which shifted to 1626 cm^{-1} in the composite. This may be attributed to the presence of carboxylate ion and an amide group. In both spectra, different characteristic sharp peaks were also observed between 1538 and 1377 cm^{-1} which may be assigned to the –C=C in the aromatic rings, asymmetric stretching (C–N) mode in addition to the bending vibrations of the methyl and methylene groups of fatty acids. The C–O–C, C–C, and carboxylic group (C–O) stretching vibrations were identified

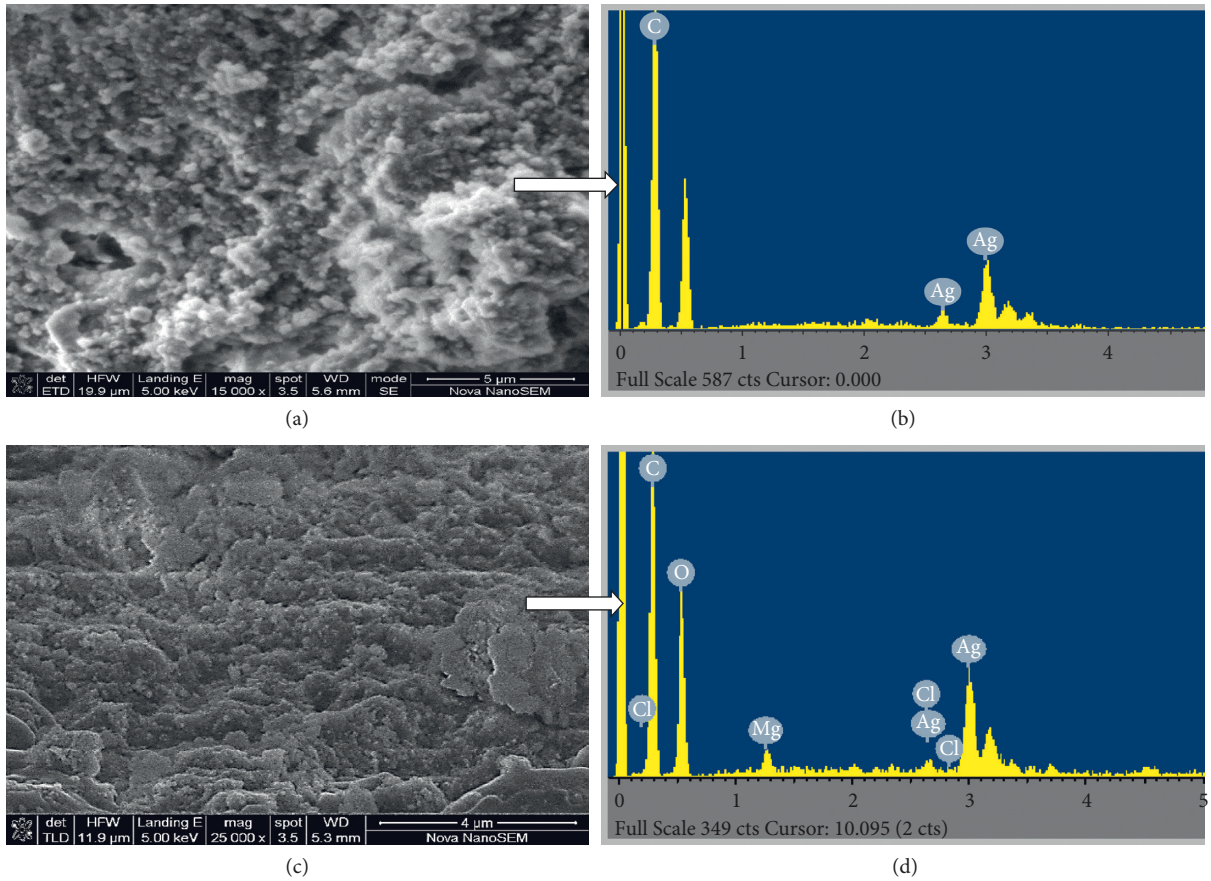

FIGURE 4: SEM images of biosynthesized (a) AgNps; (b) EDAX spectra of AgNps; (c) Ag-MgO nanocomposite; (d) EDAX spectra of Ag-MgO nanocomposite.

at 1238, 1156, and 1032 cm^{-1} bands, respectively. The absorption peaks in the region between 487–677 cm^{-1} are attributed to Mg–O–Mg compounds [45, 46], and from the spectrum of CPAgMgO, it shows Mg–O–Mg deformation of the Mg–O absorption band at 540 cm^{-1} [47]. The presence and interaction of the above bands in *C. paradisi* peel extracts indicate that the bioactive compounds were presumed to act as reducing, capping, and stabilizing agents for the biosynthesized Ag-MgO nanocomposite.

3.1.3. Surface Morphology. The resulting morphological characteristic images (SEM and TEM) with associated EDAX spectra for the biosynthesized Ag and Ag-MgO nanomaterials using the peel extract of *C. paradisi* are shown in Figures 4 and 5. The SEM micrograph of AgNps (Figure 4(a)) shows well spherically and uniformly dispersed nanoparticles, whereas the Ag-MgO composite nanoparticles image (Figure 4(b)) displayed an agglomeration of layered clustered particles. It is polydispersed and crystalline in nature. The corresponding elemental compositions suggesting the formation of the AgNps and Ag-MgO nanocomposite are depicted in Figures 4(b) and 4(d), respectively. The observed agglomeration in the composite may be due to higher amounts of organic moieties acting as the capping and stabilizing agent in the biomass of the *C. paradisi* peel extracts. In addition, the polarity and electrostatic attraction of the attached MgO nanoparticles in the composite may also result in the aggregation [48].

Figure 5 shows the morphology, shape, and particle size distribution of the biosynthesized AgNPs and Ag-MgO nanomaterial through the TEM micrograph. The TEM images (Figures 5(a)–5(c)) of *C. paradisi* peel extract-mediated synthesized AgNps and Ag-MgO composite clearly show that the particles are uniformly dispersed and mostly spherical in shape with a particle size of 14.84 nm and 11.92 nm, respectively. Figures 5(b) and 5(c) revealed the stabilization and distribution of the embedded-layered core-shell interaction between the Ag and MgO in the biosynthesized composite. The spherical shaped appearance and the sizes are well in line with the shape of the UV-visible plasmon resonance band established during the cavitation process at high intensities of exposure resulting in the conversion of larger particle sizes to smaller sizes. The images from the different scale bars (Figures 5(b) and (c)) clearly show the embedment of the bilateral core-shell interaction.

3.1.4. XRD Pattern. The X-ray diffraction patterns of Ag-MgO nanocomposite, MgO, and Ag nanoparticles

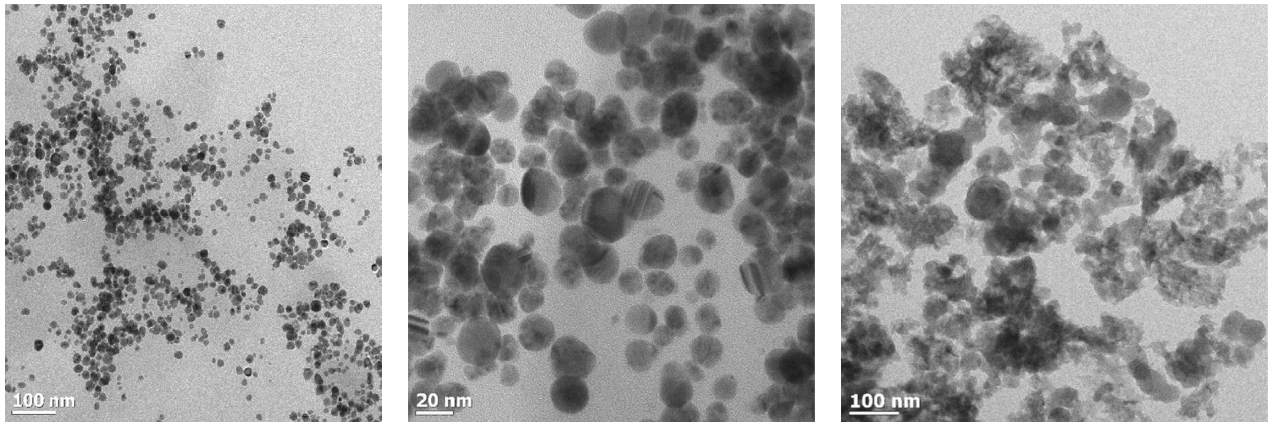

(a) (b) (c)

Figure 5: TEM micrograph. (a) AgNps; (b) scale bar Ag-MgO nanocomposite image at 20 nm; (c) Ag-MgO at 100 nm.

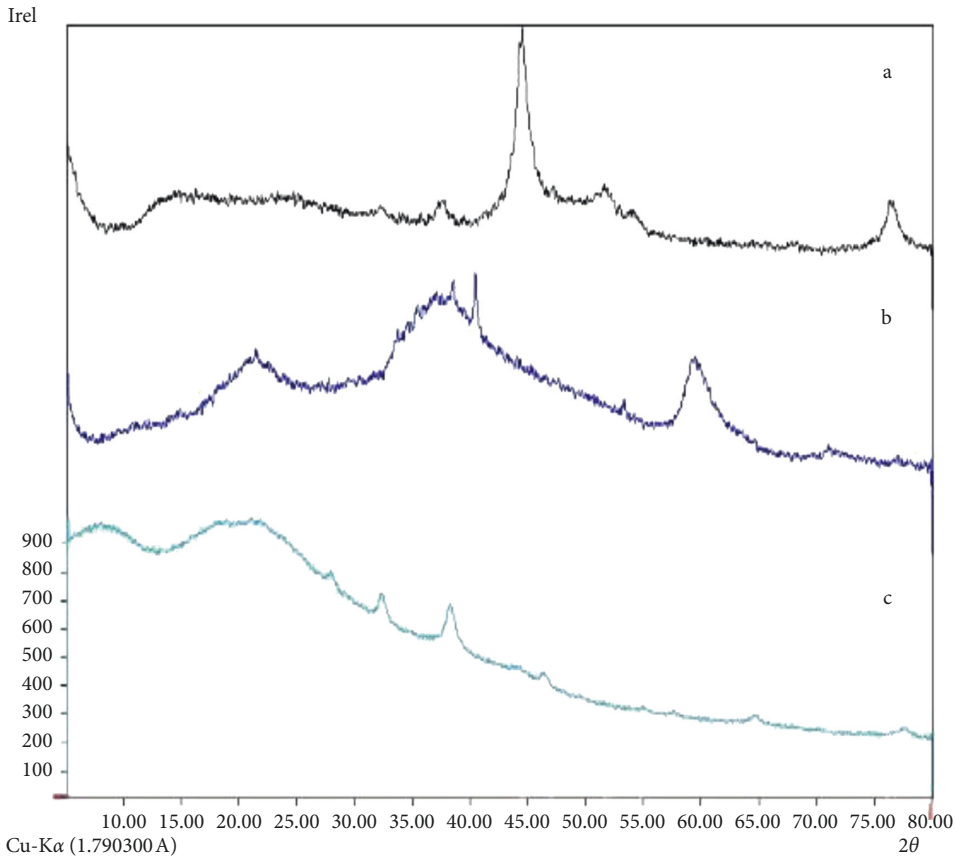

Figure 6: XRD diffractogram of biosynthesized (a) Ag-MgO nanocomposite, (b) MgO, and (c) Ag.

synthesized using aqueous *C. paradisi* peel extracts over a range of 20–80° using Cu-K radiation with their corresponding peak lists are shown in Figure 6. The nanocomposite material showed major predominant consistent reflection peaks at 2θ values between the range (20–80°) differently indexed to {111}, {200}, {202}, {311}, and {222} assigned to cubical crystal planes of Ag (reference code: 96-901-2962), together with an extended reflection labelled pattern {420} associated with the cubical system phase of MgO (reference code: 96-901-3264) which shifted to a higher prominent 2θ value deposited on Ag-MgO plane lattice interaction. Silver-magnesium (0.8/0.2) planer lattice (reference code: 96-150-9046) was also detected, thus providing confirmation of the composite nature of the material with a cubical crystal lattice network.

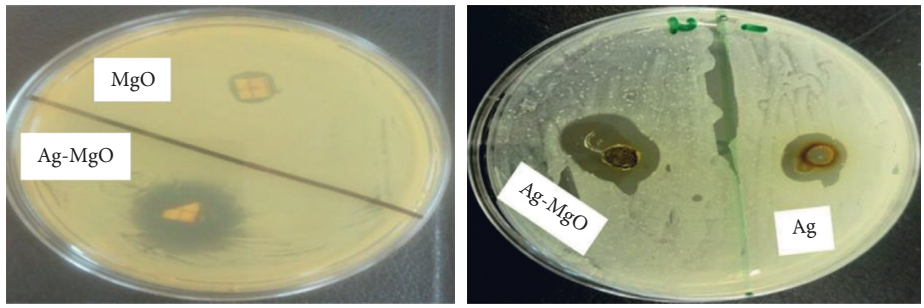

Figure 7: Antibacterial activity of biosynthesized Ag, MgO, and Ag-MgO against *E. coli*.

Table 1: Antibacterial activity.

Methods	MgO	Ag	Ag-MgO
Well diffusion assay (mm)	9	14	22
MIC (μg/mL)	80	40	20

3.1.5. Antibacterial Activity. The agar well diffusion and minimum inhibitory concentration experiments were conducted on MgO nanoparticle and Ag-MgO nanocomposite to perform a qualitative antimicrobial screening. Clear inhibition zones of varying diameters appeared against the Gram-negative bacteria *Escherichia coli* from both nanoparticles with Ag-MgO showing a wider antibacterial activity on the bacterial strain as shown in Figure 7. Ag-MgO composite exhibited a higher level of antibacterial potential on *E. coli* with 22 mm zone of inhibition in comparison with the Ag and MgO nanoparticle (Table 1). In addition to visual readings from the agar well, the viability of *E. coli* was subjected to different concentrations of the nanocomposite. As shown in Table 1, minimum inhibitory concentration (MIC) values of 80, 40, and 20 μg/mL was recorded for MgO, Ag, and Ag-MgO, respectively. The lowest concentration at which the composite showed growth inhibition was recorded as the minimum inhibitory concentration. Studies have shown that the toxicity effects at different MIC values depend on the type of bacterial strains, precursor concentration, methods of preparation, and capping agents [49–51].

Although the inactivation mechanism of action of nanoparticles against microbes has been a major debate, studies have shown that bacterial inactivation appears to be driven by the toxicity of release of metal ions as well as the generation of intracellular reactive oxygen species (ROS) upon exposure of the bacterial cells to such nanomaterials amongst other factors [52–55]. Consequently, antimicrobial potency of any material will depend on the ability to disrupt the microbial cell membrane damaging its membrane properties, permeability, and the collapsing of its respiratory functions resulting in the cell death [29].

As illustrated in Figure 8, the time-dependent releases of metal ions from *C. paradisi* peel extracts biosynthesized Ag-MgO nanocomposite were examined. Both Ag and Mg ions release were affected by time and rate of dissolution; metal ions release increases as the time progresses (Figure 8). Although the release of Mg ions is in higher concentration than the Ag ion throughout the process, both concentrations at the highest time interval (Ag ion (2.7 ppb) and Mg ions

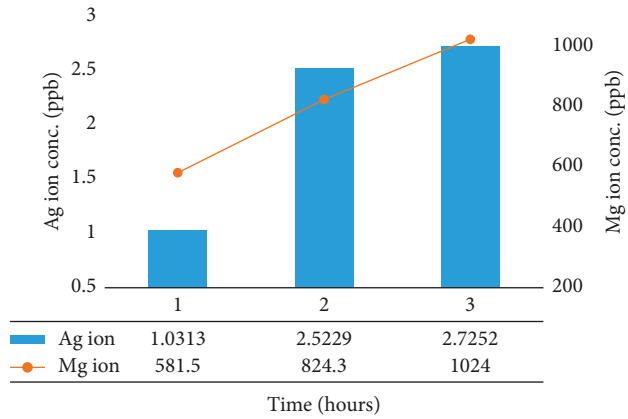

Figure 8: Time-dependent metal ions release from biosynthesized Ag-MgO nanocomposite.

(1027 ppb)) are lower than the observed minimum inhibitory concentration (MIC) (Table 1). These results suggested that the MIC value does not correlate with the mode of action of the antimicrobial activity of the Ag-MgO composite and the release of these metal ions against *Escherichia coli*. Consequently, there is a possibility that the bacterial susceptibility of this Ag-MgO nanocomposite does not only rely on the interaction of metal ions with the cell wall structures of Gram-negative bacteria genome but are also dependent on the solution pH, cellular enzymes, and biochemical events in producing intracellular reactive oxygen species (ROS) from the composite surface [15, 56, 57]. Furthermore, other factors that may be associated with microbial cell death by this nanocomposite could be attributed to its size, structure, and surface properties of the composite since smaller particles with larger surface area possess the affinity for interaction, giving more bactericidal effect than the larger particles [15, 58]. Moreover, the Ag-MgO nanocomposite antibacterial activity may also depend on the reducing and capping agents used in the synthesis route [59]. Therefore, the *C. paradisi* peel extracts used in the synthesis of Ag-MgO may have contributed to the antimicrobial activity due to the different functional phytochemical species in the peel segment, which account for the bioactivity [32, 60].

4. Conclusion

This study integrates biomediated microwave and ultrasonic simple and rapid synthetic methods using an aqueous peel

extract of the *Citrus paradisi* fruit as the reducing, capping, and stabilizing agent for synthesis of Ag-MgO nanocomposite. The presence of the phytochemicals in the extract was responsible for the rate of bioreduction leading to the formation of the composites, thus serving as an alternative to the chemical and physical synthesis route. Surface plasmon resonance nucleation growth of AgNps was observed at 410 and 440 nm upon microwave exposure, which shifted to 378 nm band upon integrating with MgO shell, which displayed an absorption band at 290 nm, confirming the presence of a bilayered Ag-MgO core-shell synergy. Surface modifications and composition of the nanocomposite showed a spherical and uniformly distributed nanocomposite with an average crystalline size of 11.92 nm. The biosynthesized Ag-MgO nanocomposite exhibited an enhanced antibacterial activity than MgO nanoparticles, proving to be a potential material against common pathogens in water treatment.

Data Availability

The data used to support the findings of this study have not been made available because of the collaboration agreements covering the research.

Conflicts of Interest

The authors declare no conflicts of interest.

Acknowledgments

The authors would like to acknowledge the financial support from USAID-PEER Cycle 6 (Award no: AID-OAA-A-11-00012); National Research Foundation (Grant no: 114726); University of Venda, South Africa (RPC Grant no: SES/17/ERM/03); and Mintek, South Africa.

References

[1] WHO/UNICEF JMP (Joint Monitoring Programme for Water Supply and Sanitation), *JMP Rapid Assessment on Drinking-Water Quality Pilot Report 2010*, WHO/UNICEF, Geneva, Switzerland/New York, NY, USA, 2010.

[2] W. Hijnen, E. Beerendonk, and G. J. Medema, "Inactivation credit of UV radiation for viruses, bacteria and protozoan (oo) cysts in water: a review," *Water Research*, vol. 40, no. 1, pp. 3–22, 2006.

[3] S. D. Emelita Asuncion, H. Ching-Shan, O. M. Rose Marie, and L. Ming-Chun, "Zinc oxide nanoparticles for water disinfection," *Sustainable Environment Research*, vol. 28, no. 2, pp. 47–56, 2018.

[4] V. K. Sharma, R. A. Yngard, and Y. Lin, "Silver nanoparticles: green synthesis and their antimicrobial activities," *Advances in Colloid and Interface Science*, vol. 145, no. 1-2, pp. 83–96, 2009.

[5] H. J. Lee, S. J. Yeo, and S. H. Jeong, "Antibacterial effect of nanosized silver colloidal solution on textile fabrics," *Journal of Materials Science*, vol. 38, no. 10, pp. 2199–2204, 2003.

[6] T. Prathna, A. Mukherjee, A. M. Raichur, L. Mathew, and N. Chandrasekaran, *Biomimetic Synthesis of Nanoparticles: Science, Technology & Applicability*, INTECH Open Access Publisher, Rijeka, Croatia, 2010.

[7] J. L. Gardea Torresdey, G. L. Parsons, E. Gomez et al., "Formation and growth of Au nanoparticles inside live Alfalfa plant," *Nano Letters*, vol. 2, no. 4, pp. 397–401, 2002.

[8] M. Rafique, I. Sadaf, M. Shahid Rafique, and M. Bilal Tahir, "A review on green synthesis of silver nanoparticles and their applications," *Artificial Cells, Nanomedicine, and Biotechnology*, vol. 45, no. 7, pp. 1272–1291, 2016.

[9] X. Zhu, D. Wu, W. Wang et al., "Highly effective antibacterial activity and synergistic effect of Ag-MgO nanocomposite against *Escherichia coli*," *Journal of Alloys and Compounds*, vol. 684, pp. 282–290, 2016.

[10] Z.-X. Tang and B.-F. Lv, "MgO nanoparticles as antibacterial agent: preparation and activity," *Brazilian Journal of Chemical Engineering*, vol. 31, no. 3, pp. 591–601, 2014.

[11] A. Monzavi, S. Eshraghi, R. Hashemian, and F. Momen-Heravi, "In vitro and ex vivo antimicrobial efficacy of nano-MgO in the elimination of endodontic pathogens," *Clinical Oral Investigations*, vol. 19, no. 2, pp. 349–356, 2015.

[12] S. Schultz, D. R. Smith, J. J. Mock, and D. A. Schultz, "Single-target molecule detection with nonbleaching multicolor optical immunolabels," *Proceedings of the National Academy of Sciences*, vol. 97, no. 3, pp. 996–1001, 2000.

[13] C. Krishnaraj, E. G. Jagan, S. Rajasekar, P. Selvakumar, P. T. Kalaichelvan, and N. Mohan, "Synthesis of silver nanoparticles using *Acalypha indica* leaf extracts and its antibacterial activity against water-borne pathogens," *Colloids and Surfaces B: Biointerfaces*, vol. 76, no. 1, pp. 50–56, 2010.

[14] G. Franci, A. Falanga, S. Galdiero et al., "Silver nanoparticles as potential antibacterial agents," *Molecules*, vol. 20, no. 5, pp. 8856–8874, 2015.

[15] Y. H Leung, A. Ng, X. Xu et al., "Mechanisms of antibacterial activity of MgO: non-ROS mediated toxicity of MgO nanoparticles towards *Escherichia coli*," *Small*, vol. 10, no. 6, pp. 1171–1183, 2014.

[16] G. Sharma and N. D. Jasuja, "Phytoassisted synthesis of magnesium oxide nanoparticles by *Swertia chirayita*," *Journal of Taibah University for Science*, vol. 11, no. 3, pp. 471–477, 2016.

[17] R. D. Rashmi, M. U. Iohborlang, K. R. Prasanta, D. Bodhaditya, B. Saumen, and S. Lokendra, "Defluoridation of water using nano-magnesium oxide," *Journal of Experimental Nanoscience*, vol. 9, no. 5, pp. 512–524, 2014.

[18] Y. Cai, D. Wu, X. Zhu et al., "Sol-gel preparation of Ag-doped MgO nanoparticles with high efficiency for bacterial inactivation," *Ceramics International*, vol. 43, no. 1, pp. 1066–1072, 2017.

[19] Y. Cai, C. Li, D. Wu et al., "Highly active MgO nanoparticles for simultaneous bacterial inactivation and heavy metal removal from aqueous solution," *Chemical Engineering Journal*, vol. 312, pp. 158–166, 2017.

[20] O. V. Kharissova, H. R. Dias, B. I. Kharisov, B. O Pe´rez, and V. M. J. Pe´rez, "The greener synthesis of nanoparticles," *Trends in Biotechnology*, vol. 31, no. 4, pp. 240–248, 2013.

[21] G. Singhal, R. Bhavesh, K. Kasariya, A. R. Sharma, and R. P Singh, "Biosynthesis of silver nanoparticles using *Ocimum sanctum* (Tulsi) leaf extract and screening its antimicrobial activity," *Journal of Nanoparticle Research*, vol. 13, no. 7, pp. 2981–2988, 2011.

[22] M. N. Nadagouda, G. Hoag, J. Collins, and R. S. Varma, "Green synthesis of Au nanostructures at room temperature using biodegradable plant surfactants," *Crystal Growth and Design*, vol. 9, no. 11, pp. 4979–4983, 2009.

[23] M. Shah, D. Fawcett, S. Sharma, S. K. Tripathy, and G. E. J. Poinern, "Green synthesis of metallic nanoparticles via

biological entities," *Materials*, vol. 8, no. 11, pp. 7278–7308, 2015.

[24] N. John Sushma, D. Prathyusha, G. Swathi et al., "Facile approach to synthesize magnesium oxide nanoparticles by using *Clitoria ternatea*—characterization and in vitro antioxidant studies," *Applied Nanoscience*, vol. 6, no. 3, p. 437, 2016.

[25] L. Arangasamy and V. Munusamy, "Tapping the unexploited plant resources for the synthesis of silver nanoparticles," *African Journal of Biotechnology*, vol. 7, no. 17, pp. 3162–3165, 2008.

[26] H. Genuino, H. Huang, E. Njagi, L. Stafford, and S. L. Suib, "A review of green synthesis of nanophase inorganic materials for green chemistry applications," *Handbook of Green Chemistry*, vol. 8, no. 8, pp. 217–244, 2012.

[27] E. O. Dare, C. O. Oseghale, A. H. Labulo et al., "Green synthesis and growth kinetics of nanosilver under biodiversified plant extracts influence," *Journal of Nanostructure in Chemistry*, vol. 5, no. 1, pp. 85–94, 2015.

[28] S. N John and D. Prathyusha, "Facile approach to synthesize magnesium oxide NPs by using *Clitoria ternatea*-characterization and in vitro antioxidant studies," *Applied Nanoscience*, vol. 6, no. 3, p. 895, 2016.

[29] K. Ramanujam and M. Sundrarajan, "Antibacterial effects of biosynthesized MgO nanoparticles using ethanolic fruit extract of *Emblica officinalis*," *Journal of Photochemistry and Photobiology B: Biology*, vol. 141, pp. 296–300, 2014.

[30] S. Yusof, H. Mohd Ghazali, and G. Swee King, "Naringin content in local citrus fruits," *Food Chemistry*, vol. 37, no. 2, pp. 113–121, 1990.

[31] V. Andrea, N. Nadia, R. M. Teresa, and A. Andrea, "Analysis of some Italian lemon liquors (*Limoncello*)," *Journal of Agricultural Food Chemistry*, vol. 51, no. 17, pp. 4978–4983, 2003.

[32] S. Gorinstein, O. Martın-Belloso, Y. S. Park et al., "Comparison of some biochemical characteristics of different citrus fruits," *Food Chemistry*, vol. 74, no. 3, pp. 309–315, 2001.

[33] C. J. Dillard and J. B. German, "Phytochemicals: nutraceuticals and human health," *Journal of the Science of Food and Agriculture*, vol. 80, no. 12, pp. 1744–1756, 2000.

[34] G. K. Jayaprakasha, B. Girennavar, and B. S. Patil, "Radical scavenging activities of RioRed grapefruits and Sour orange fruit extracts in different *in vitro* model systems," *Journal of Bioresource Technology*, vol. 99, no. 10, pp. 4484–4494, 2008.

[35] S. Horikoshi and N. Serpone, *Microwaves in Nanoparticle Synthesis–Fundamentals and Applications*, Wiley-VCH Verlag GmbH, Weinheim, Germany, 2013.

[36] S. G. Babu, B. Neppolian, and M. Ashokkumar, "Ultrasound-assisted synthesis of nanoparticles for energy and environmental applications," in *Handbook of Ultrasonics and Sonochemistry*, M. Ashokkumar, Ed., Springer, Singapore, 2015.

[37] A Samie, C. L. Obi, P. O. Bessong, and L. Namrita, "Activity profiles of fourteen selected medicinal plants from Rural Venda communities in South Africa against fifteen clinical bacterial species," *African Journal of Biotechnology*, vol. 4, no. 12, pp. 1443–1451, 2005.

[38] E. Elias Emeka, O. C. Ojiefoh, C. Aleruchi et al., "Evaluation of antibacterial activities of silver nanoparticles green-synthesized using pineapple leaf (*Ananas comosus*)," *Micron*, vol. 57, pp. 1–5, 2014.

[39] K. Anandalakshmi, J. Venugobal, and V. Ramasamy, "Characterization of silver nanoparticles by green synthesis method using *Pedalium murex* leaf extract and their antibacterial activity," *Applied Nanoscience*, vol. 6, no. 3, pp. 399–408, 2016.

[40] L.-Y. Meng, B. Wang, M.-G. Ma, and K.-L. Lin, "The progress of microwave-assisted hydrothermal method in the synthesis of functional nanomaterials," *Materials Today Chemistry*, vol. 1-2, pp. 63–83, 2016.

[41] H. M. Santos, C. Lodeiro, and J. L. Capello-Martinez, "The power of ultrasound," in *Ultrasound in Chemistry: Analytical Applications*, J. L. Capello-Martinez, Ed., pp. 1–15, Wiley-Vch Verlag GmbH & Co. KGaA, Weinheim, Germany, 2009.

[42] S.S. Sawant, A. C. Anil, V. Krishnamurthy et al., "Effect of hydrodynamic cavitation on zooplankton: a tool for disinfection," *Biochemical Engineering Journal*, vol. 42, no. 3, pp. 320–328, 2008.

[43] J. Li and A. R. Barron, "Fourier transform infrared spectroscopy of metal ligand complexes," OpenStax-CNX module: m3 4660, 2010.

[44] B. Kumar, K. Smita, L. Cumbal, and A. Debut, "Biogenic synthesis of iron oxide nanoparticles for 2-arylbenzimidazole fabrication," *Journal of Saudi Chemical Society*, vol. 18, no. 4, pp. 364–369, 2014.

[45] G. Marquis, B. Ramasamy, B. Sarkar, and A. P. Munusamy, "Evaluation of antibacterial activity of plant mediated CaO nanoparticles using *Cissus quadrangularis* extract," *Journal of Photochemistry and Photobiology B: Biology*, vol. 155, pp. 28–33, 2016.

[46] W. Wang, X. Qiao, and J. Chen, "The role of acetic acid in magnesium oxide preparation via chemical precipitation," *Journal of the American Ceramic Society*, vol. 91, no. 5, pp. 697–1699, 2008.

[47] S. Balamurugan, L. Ashna, and P. Parthiban, "Synthesis of nanocrystalline MgO particles by combustion followed by annealing method using hexamine as a fuel," *Journal of Nanotechnology*, vol. 2014, Article ID 841803, 6 pages, 2014.

[48] T. Ponnaiah and A. Ramasamy, "Synthesis of hierarchical structured MgO by sol-gel method," *Journal of Nanotechnology Bulletin*, vol. 2, no. 2, pp. 130–106, 2013.

[49] M. E. Velazquez-Meza, M. Hernández-Salgado, and M. A. Sánchez-Alemán, "Evaluation of the antimicrobial activity of a super oxidized solution in clinical isolates," *Microbial Drug Resistance*, vol. 21, no. 4, pp. 367–372, 2015.

[50] J. Mittal, R. Jain, and M. M. Sharma, "Phytofabrication of silver nanoparticles using aqueous leaf extract of *Xanthium strumerium* L. and their bactericidal efficacy," *Advances in Natural Sciences: Nanoscience and Nanotechnology*, vol. 8, no. 2, article 025011, 2017.

[51] P. Gong, H. Li, X. He et al., "Preparation and antibacterial activity of Fe_3O_4@ Ag nanoparticles," *Nanotechnology*, vol. 18, no. 28, article 285604, 2007.

[52] H. J. Park, J. Y. Kim, J. Kim et al., "Silver-ion-mediated reactive oxygen species generation affecting bactericidal activity," *Water Research*, vol. 43, no. 4, pp. 1027–1032, 2009.

[53] W. Zhang, Y. Yao, N. Sullivan, and Y. Chen, "Modeling the primary size effects of citrate-coated silver nanoparticles on their ion release kinetics," *Environmental Science and Technology*, vol. 45, no. 10, pp. 4422–4428, 2011.

[54] M. Horie, K. Fujita, H. Kato et al., "Association of the physical and chemical properties and the cytotoxicity of metal oxide nanoparticles: metal ion release, adsorption ability and specific surface area," *Metallomics*, vol. 4, no. 4, pp. 50–360, 2012.

[55] K. Krishnamoorthy, J. Y. Moon, H. B. Hyun, S. K. Cho, and S. J. Kim, "Mechanistic investigation on the toxicity of MgO nanoparticles toward cancer cells," *Journal of materials chemistry*, vol. 22, no. 47, pp. 24610–24617, 2012.

[56] N. Durán, M. Durán, M. Bispo de Jesús, A. B. Seabra, W. J. Fávaro, and G. Nakazato, "Silver nanoparticles: a new view on mechanistic aspects on antimicrobial activity," *Nanomedicine: Nanotechnology, Biology and Medicine*, vol. 12, no. 3, pp. 789–799, 2016.

[57] K. Krishnamoorthy, G. Manivannan, S. J. Kim, K. Jeyasubramanian, and M. Premanathan, "Antibacterial activity of MgO nanoparticles based on lipid peroxidation by oxygen vacancy," *Journal of Nanoparticle Research*, vol. 14, no. 9, p. 1063, 2012.

[58] K. R. Raghupathi, R. T. Koodali, and A. C. Manna, "Size-dependent bacterial growth inhibition and mechanism of antibacterial activity of zinc oxide nanoparticles," *Langmuir*, vol. 27, no. 7, pp. 4020–4028, 2011.

[59] P. Kuppusamy, M. M. Yusoff, G. P. Maniam, and N. Govindan, "Biosynthesis of metallic nanoparticles using plant derivatives and their new avenues in pharmacological applications–an updated report," *Saudi Pharmaceutical Journal*, vol. 24, no. 4, pp. 473–484, 2016.

[60] S. A. Aromal and D. Philip, "Green synthesis of gold nanoparticles using Trigonella foenum-graecum and its size-dependent catalytic activity," *Spectrochimica Acta Part A: Molecular and Biomolecular Spectroscopy*, vol. 97, pp. 1–5, 2012.